Journal of Power Sources 196 (2011) 768–775

Contents lists available at ScienceDirect

Journal of Power Sources

journal homepage: www.elsevier.com/locate/jpowsour

Electrolytic Sn/Li_2O coatings for thin-film lithium ion battery anodes

Ching-Fei Li [a], Wen-Hsien Ho [b], Chi-Sheng Jiang [b], Chien-Chang Lai [a], Ming-Jia Wang [a], Shiow-Kang Yen [a,*]

[a] Department of Materials Science and Engineering, National Chung Hsing University, Taichung 40227, Taiwan
[b] Taiwan Textile Research Institute, Taipei 23674, Taiwan

ARTICLE INFO

Article history:
Received 6 April 2010
Received in revised form 15 July 2010
Accepted 21 July 2010
Available online 6 August 2010

Keywords:
Electrolytic deposition
Tin/lithium oxide
Lithium battery anode

ABSTRACT

Sn/Li_2O composite coatings on stainless steel substrate, as anodes of thin-film lithium battery are carried out in $SnCl_2$ and $LiNO_3$ mixed solutions by using cathodic electrochemical synthesis and subsequently annealed at 200 °C. Through cathodic polarization tests, three major regions are verified: (I) $O_2 + 4H^+ + 4e^- \rightarrow 2H_2O$ (~0.25 to −0.5 V), (II) $2H^+ + 2e^- \rightarrow H_2$, $Sn^{2+} + 2e^- \rightarrow Sn$, and $NO_3^- + H_2O + 2e^- \rightarrow NO_2^- + 2OH^-$ (−0.5 to −1.34 V), and (III) $2H_2O + 2e^- \rightarrow H_2 + 2OH^-$ (−1.34 to −2 V vs. Ag/AgCl). The coated specimens are characterized by X-ray diffraction (XRD), scanning electron microscopy (SEM), X-ray photoelectron spectroscopy (XPS), cyclic voltammetry (CV), and charge/discharge tests. The nano-sized Sn particles embedded in Li_2O matrix are obtained at the lower part of region II such as −1.2 V, while the micro-sized Sn with little Li_2O at the upper part, such as −0.7 V. Charge/discharge cycle tests elucidated that Sn/Li_2O composite film showed better cycle performance than Sn or SnO_2 film, due to the retarding effects of amorphous Li_2O on the further aggregation of Sn particles. On the other hand, the one tested for cut-off voltage at 0.9 V (vs. Li/Li^+) is better than those at 1.2 and 1.5 V since the incomplete de-alloy at lower cut-off voltage may inhibit the coarsening of Sn particles, revealing capacity 587 mAh g^{-1} after 50 cycle, and capacity retention ratio C50/C2 81.6%, higher than 63.5% and 49.1% at 1.2 and 1.5 V (vs. Li/Li^+), respectively.

1. Introduction

The light, thin, short, and small devices with environmental protection and safety should be demanded for 3C (communication, computer, and electronics consumer products) in the 21st century. Therefore, developing rechargeable battery technologies to achieve higher energy density and specific energy is quite urgent. Much research has been undertaken for new anode materials in place of carbon (theoretical maximum capacity of 372 mAh g^{-1}) to improve energy density for rechargeable lithium-ion batteries [1]. Since FUJI Photo-film published patents [2,3] for the use of tin-based composite oxide (TCO) as an alternative anode material for lithium-ion batteries in 1995, a lasting interest in tin alloys and compounds has grown. The Li-ion anodes derived from tin-based materials received considerable interest because the theoretical capacity of the tin-based material is 994 mAh g^{-1} and it can easily store 50% reversible lithium more than the carbon-based lithium intercalation materials in principle [4–10]. However, some serious problems exist in tin-based materials. It was reported that lithium first reacts irreversibly with tin oxides in a manner consistent with the formation of amorphous Li_2O and Sn, followed by the alloying of Li with Sn in the manner suggested by the Li–Sn phase diagram [4]. To mitigate the irreversible capacity associated with tin oxides, metallic electrodes such as metallic tin [11] or other tin composites [12,13] have been employed as negative electrode. However, another main drawback of metallic tin is the drastic volume variation (up to about 300%) due to lithium insertion/removal into/from host materials during the charge/discharge cycles. To solve these problems, some researchers have reported that the reduction of Sn particle sizes and multi-phases has enhanced the cycling performance [14–19]. Also, it has been pointed out that the Li_2O produced from the reduction forms a homogeneous matrix which serves as a buffer to accommodate the volume change of Li–Sn alloy/de-alloy reaction [4]. Recently, the Sn/Li_2O layered structure or Sn/Li_2O co-sputtered thin film [20,21] prepared by RF magnetron sputtering system has showed better cycling behavior than pure Sn or SnO_2.

In this study, the electrolytic co-deposition of Sn/Li_2O thin films on stainless steel was conducted in the $SnCl_2$ and $LiNO_3$ mixed aqueous solution for anodes in lithium ion thin-film batteries. Cathodic polarization tests were carried out to investigate the electrochemical reactions and the better deposition parameters. The coated specimens were further characterized by X-ray diffraction (XRD) for crystal structure, scanning electron microscopy (SEM) for surface morphology, X-ray photoelectron spectroscopy (XPS) for chemical bonding, cyclic voltammetry (CV) for electrochemical properties, and charge/discharge test for capacity variations.

* Corresponding author. Tel.: +886 4 22852953; fax: +886 4 22857017.
E-mail address: skyen@dragon.nuch.edu.tw (S.-K. Yen).

0378-7753/$ – see front matter © 2010 Elsevier B.V. All rights reserved.
doi:10.1016/j.jpowsour.2010.07.068

Table 1
Molarity (mol L^{-1}), pH, O_2 (mg L^{-1}), conductivity of solution (κ), and the first, second, third, and fourth limiting current densities of polarization curves in aqucous aerated 1 mM $SnCl_2$ (solution A), 0.5 mM $SnCl_2$ (solution B), 1 mM $SnCl_2$ deaerated with N_2 (solution C), and deionized water with pH adjusted by adding HCl (solution D), and aerated mixture of 1 mM $SnCl_2$ and 10 mM $LiNO_3$ (solution E).

Solutions	pH	O_2% (mg L^{-1})	κ (μS cm^{-1})	Limiting current density (A cm^{-2})			
				Region I	Region II	Region III	Region IV
A	2.95	6.25	544	5.49×10^{-7}	1.09×10^{-4}	1.95×10^{-4}	1.14×10^{-3}
B	3.68	6.07	277	4.65×10^{-7}	4.57×10^{-5}	6.35×10^{-5}	6.76×10^{-4}
C	2.96	0.18	122	1.48×10^{-7}	1.09×10^{-4}	2.39×10^{-4}	1.29×10^{-3}
D	2.92	6.17	396	5.12×10^{-7}	7.36×10^{-5}	7.36×10^{-5}	8.32×10^{-4}
E	2.54	6.34	1611	6.61×10^{-7}	1.74×10^{-4}	4.89×10^{-4}	3.26×10^{-3}

2. Experimental

2.1. Substrate preparation

304 stainless steel cut into 1 cm × 1 cm plate was used as a substrate for the electrolytic Sn/Li_2O deposition. All specimens were cleaned in deionized water and acetone by ultrasonic cleaner then dried at room temperature.

2.2. Cathodic polarization tests and deposition

To investigate the effect of solution concentration on the cathodic reaction, the stainless steel disks were electrochemically polarized in aerated 1 and 0.5 mM $SnCl_2{\cdot}2H_2O$ aqueous solutions assigned as solutions A and B, respectively, by EG&G Princeton Applied Research 263A Potentiostat M352 software. To investigate the effect of O_2 and H^+ concentrations on cathodic reaction, the polarization tests were also conducted in as-prepared 1 mM $SnCl_2$ solution deaerated by N_2 purging, assigned as solution C, and in deionized water with pH adjusted to 2.95 by adding HCl, assigned as solution D. To investigate the effect of LiOH deposition on the cathodic reaction, the polarization test was also conducted in the mixed of 1 mM $SnCl_2{\cdot}2H_2O$ and 10 mM $LiNO_3$ solution, assigned as solution E. The potential was swept from the equilibrium potential of the stainless steel to a final potential of −2.0 V (vs. potential of saturated Ag/AgCl), at a scanning rate of 0.167 mV s^{-1}. The details of electrochemical solutions including pH values, O_2 concentrations, and solution conductivity (κ) are also given in Table 1.

To further characterize the coated specimens, the cathodic deposition of Sn/Li_2O films on stainless steel was carried out in solution E for 40 min, at −0.7, −0.8, −0.9, −1.0, −1.1, and −1.2 V (Ag/AgCl) respectively.

2.3. XRD, SEM and TEM

The crystal structures of the as-coated, and the post-annealed at 200 and 250 °C for 3 h were analyzed by X-ray diffraction (XRD) technique in a MAC MO3X-HF diffractometer, with Cu Kα radiation (λ = 1.5418 Å), 2θ from 10° to 70°, at a scanning rate of 1° min^{-1}, a voltage of 40 kV, and a current of 30 mA. The surface morphology of the deposited samples was observed by scanning electron microscopy (SEM, JEOL model JSM-6700F). The microstructure of the Sn/Li_2O films was examined by analytical transmission electron microscopy (TEM, JEM 1200EX II).

2.4. XPS

To examine the existence of Li_2O in the coating film, X-ray photoelectron spectroscopy (XPS) measurements were performed on ESCA ULVAC-PHI 5000 system with an operating pressure of 6.7×10^{-8} Pa using Mg Kα radiation as the excitation source. Peaks were recorded with constant step energy of 0.2 eV, and pass energy of 58.7 eV. To correct possible charge-up of films by X-ray irradiation, the binding energy was calibrated using C 1s spectrum of hydrocarbon that remained in the XPS analysis chamber as a contaminant.

2.5. Electrochemical characterization

For the electrochemical measurements, two-electrode and three-electrode cells were employed with Sn/Li_2O-coated specimen as the working electrode, one lithium thin foil the reference electrode and the other one counter electrode. Prior to fabrication, all Sn/Li_2O coated specimens were dried for at least 12 hours at 80 °C and further annealing at 200 °C for 3 h in a vacuum oven. The ultimate pressure of the vacuum oven was about 0.1 MPa. The electrolyte consisted of 1 M $LiClO_4$ dissolved in a nonaqueous solution of propylene carbonate. The cells were assembled in an argon-filled glove box. First cyclic voltammetry (CV) measurement was carried out between 0.02 and 1.5 V (vs. Li/Li^+) at scanning rate of 0.5 mV s^{-1} using an EG&G model 263 potentiostat/galvanostat. The charge–discharge measurement was performed at a current density of 50 μA cm^{-2} with the cut-off voltage of 0.9, 1.2, and 1.5 V versus Li/Li^+ using a Maccor series 2000 battery tester apparatus at room temperature.

3. Results and discussion

3.1. Cathodic reaction

The polarization curves were divided into three regions, as shown in Fig. 1. The diffusion-limited current densities corresponding to region I, region II, and region III for solution A, B, C, D, and E were given in Table 1. The possible reactants of electrolytic solution

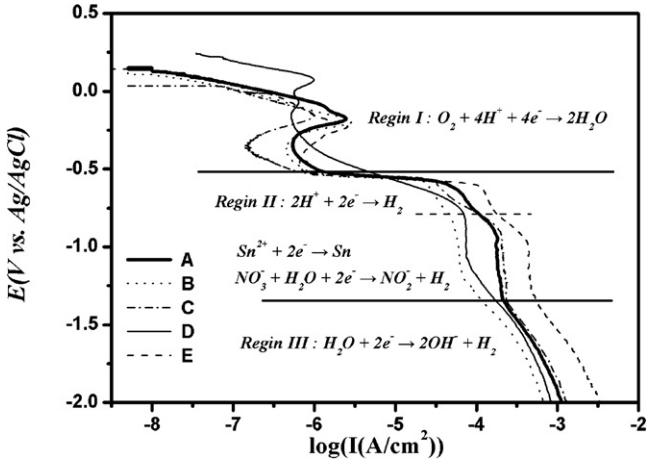

Fig. 1. Cathodic polarization curves of stainless steel in aerated 1 mM $SnCl_2$ aqueous solution (curve A), 0.5 mM $SnCl_2$ (curve B), 1 mM $SnCl_2$ deaerated with N_2 (curve C), and deionized water with pH adjusted by adding HCl (curve D), and aerated mixture of 1 mM $SnCl_2$ and 10 mM $LiNO_3$(curve E).

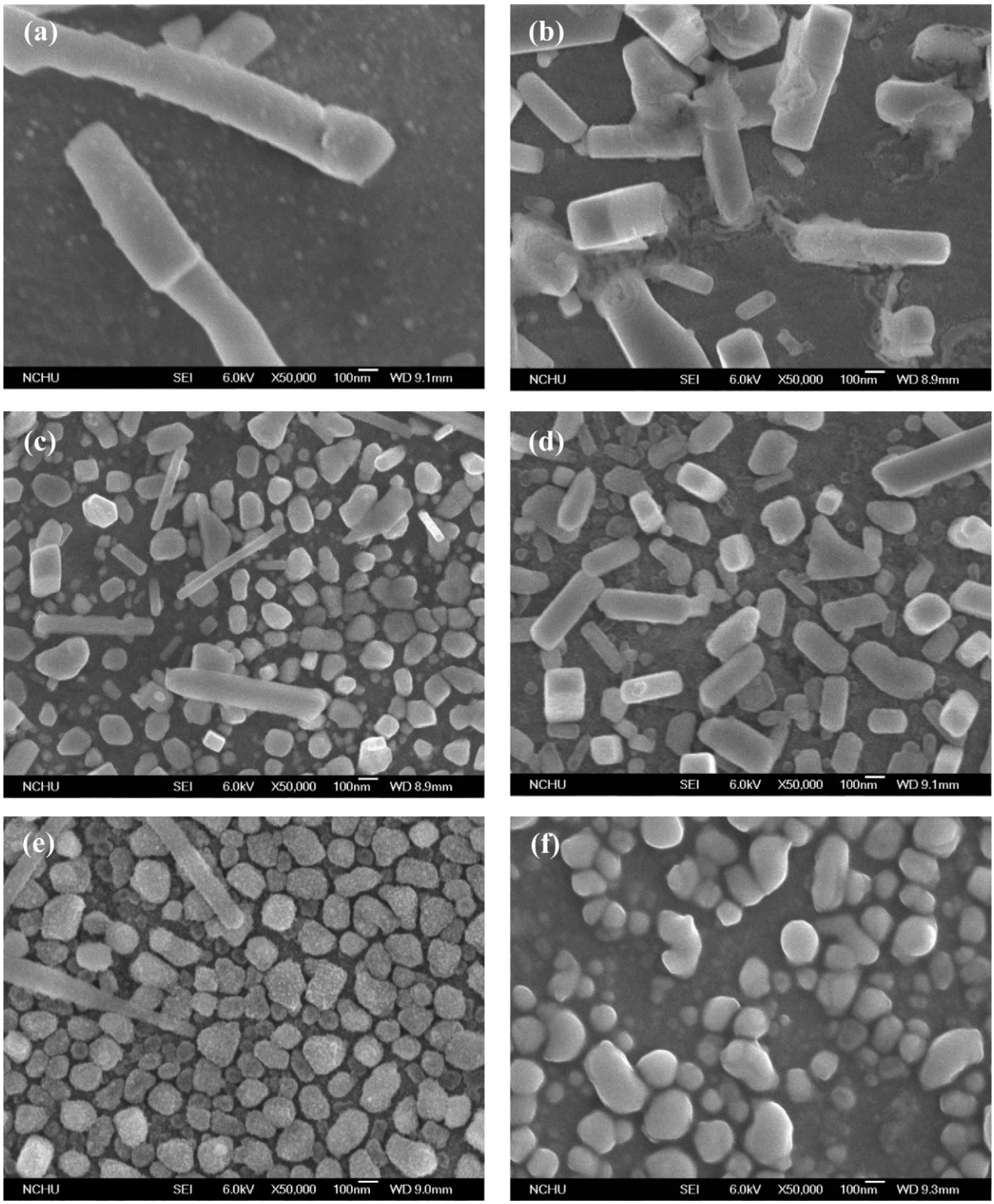

Fig. 2. FE-SEM observations of Sn/Li_2O composite films deposited at (a) −0.7, (b) −0.8, (c) −0.9, (d) −1.0, (e) −1.1, and (f) −1.2 V (Ag/AgCl) for 40 min.

should be H^+, O_2, H_2O, Sn^{2+}, and NO_3^-. The related possible cathodic reactions in the electrolytic solution was suggested as follows

$$O_2 + 4H^+ + 2e^- \rightarrow 2H_2O \qquad E = 1.032\,\text{V vs. Ag/AgCl} \tag{1}$$

$$2H^+ + 2e^- \rightarrow H_2 \qquad E = -0.197\,\text{V vs. Ag/AgCl} \tag{2}$$

$$Sn^{2+} + 2e^- \rightarrow Sn \qquad E = -0.335\,\text{V vs. Ag/AgCl} \tag{3}$$

$$H_2O + NO_3^- + 2e^- \rightarrow NO_2^- + 2OH^- \qquad E = -0.187\,\text{V vs. Ag/AgCl} \tag{4}$$

$$2H_2O + 2e^- \rightarrow H_2 + 2OH^- \qquad E = -1.025\,\text{V vs. Ag/AgCl} \tag{5}$$

Region I (~0.25 to −0.5 V)—The deaerating treatment by N_2 purging revealed the first limiting current density form 5.49×10^{-7} down to 1.48×10^{-7} A cm^{-2}, as shown in Fig. 1(curves A and C). The major change of cathodic reactant was concentration of O_2. This

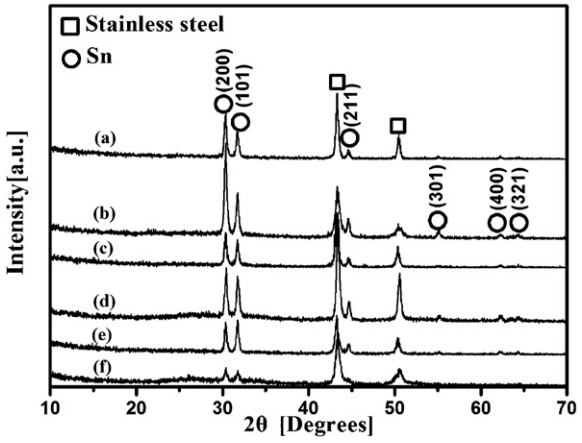

Fig. 3. XRD patterns of the samples as-deposited at (a) −0.7, (b) −0.8, (c) −0.9, (d) −1.0, (e) −1.1, and (f) −1.2 V (Ag/AgCl) for 40 min.

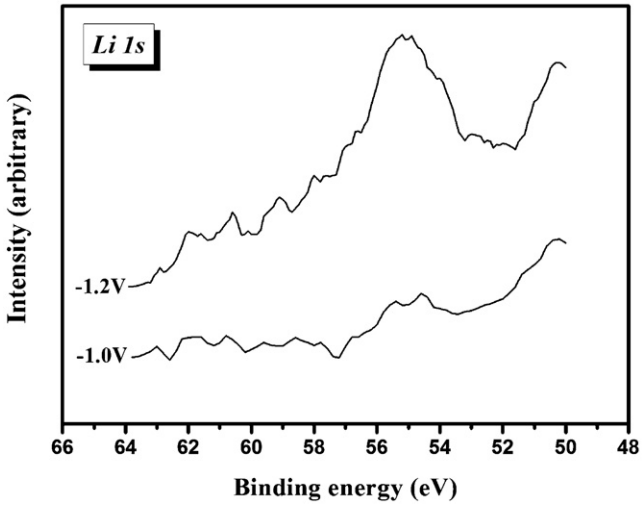

Fig. 4. XPS spectra of the Sn/Li_2O films deposited at (a) −1.0 and (b) −1.2 V (Ag/AgCl).

means that O_2 played a major role at this region. Reactions (2)–(4) could be excluded because of the positive potential region. Therefore, only reaction (1) remained the possible one and its limiting current density was controlled by diffusion rate of O_2.

Region II, the upper part (−0.5 to −0.77 V)—Once pH value was varied from 3.68 to 2.95, the limiting current density was enhanced from 4.57×10^{-5} up to 1.09×10^{-4} A cm^{-2}, as shown in Fig. 1(curves A and B). The major differences between them were reactant concentration of H^+ and Sn^{2+}. Therefore, this limiting current density is possibly linked to H^+ in reaction (2) or Sn^{2+} in reaction (3). The cathodic polarization curve in HCl (pH 2.92) as shown in Fig. 1(curve D) reveals a prominent limiting current density (4.16×10^{-5} A cm^{-2}) between −0.37 and −1 V. Compared with solution A, the only difference is Sn^{2+}. Obviously, the current density at region II of solution A was mainly caused by diffusion limit of H^+ in reaction (2) and further enhanced by reaction (3). Also, the higher current density of solution E was caused by the lower pH value and reaction (4).

Region II the lower part (−0.77 to −1.34 V)—The different limiting current densities of the lower part in region II were found for all solutions. Once the pH value was from 3.68 down to 2.92 and $SnCl_2$ concentration was from 0.5 up to 1 mM, the limiting current density was enhanced from 6.606×10^{-5} up to 1.949×10^{-4} A cm^{-2}, as shown in Fig. 1(curves A and B). These limiting current densities are possibly linked to H^+ in reaction (2) and/or Sn^{2+} in reaction (3) and NO_3^- in reaction (4). However, reaction (2) could be minor because the limiting current density of solution D (pure H_2O with HCl) is lower than solution A (1 mM $SnCl_2$) at the same pH value. This means that Sn^{2+} and NO_3^- played the major role at lower part of region II, and the limiting current density was controlled by diffusion rate of Sn^{2+} in reaction (3) and NO_3^- in reaction (4). At less negative voltage from −0.7 to −0.9 V, lower deposition efficiency was found because the potential corresponding to reactions (3) and (4) did not reach the limiting current densities. However, the deposition was found more efficient at more negative voltage such as −1.2 V, because much more OH^- ions were supplied in reaction (4) accompanied by reaction (3), and Li^+ ions migrated to the cathode to form LiOH by the following reaction

$$Li^+ + OH^- \rightarrow LiOH \quad (6)$$

LiOH was condensed into Li_2O by subsequently annealing, i.e.

$$2LiOH \rightarrow Li_2O + H_2O \uparrow \quad (7)$$

In order to deposit Sn/Li_2O composite films, therefore, the applied voltage was controlled at the lower part of region II.

Region III (−1.34 to −2 V)—The polarization curves were clearly separated in region III. A lot of hydrogen bubbles were found on the electrode surface for all solutions. Most of the hydrogen is released by reaction (5), taking place even at neutral pH. In this case current density is directly proportional to the conductivity of the solution as listed in Table 1.

3.2. Surface morphology

SEM observations of Sn/Li_2O thin films carried out at various deposition potentials are shown in Fig. 2. The coarse rod-shaped structures were observed at −0.7 and −0.8 V, as shown in Fig. 2(a) and (b). Only few heterogeneous nucleation were found on the metal substrate since the reduction rate of Sn^{2+} ions in reaction (3) did not reach the limitation yet. However, the reduction of H^+ in reaction (2) did. At more negative voltage such as −0.9 to −1.0 V, the resultant Sn film composed of rods and round particles, as shown in Fig. 2(c) and (d), due to more reduction of Sn^{2+} ions in reaction (3), as shown in Fig. 1 region II for solution E. When the deposition voltage was raised to −1.1 V, the ratio of rods structure decreased and round particles increased, as shown in Fig. 2(e). It is speculated that the nucleation rate increased faster than the growth rate, and the deposition of each layer proceeds with the formation of a large number of nuclei. The particle size is decreased with increasing applied voltage due to the nuclei overlap and growth centers impinge on each other, where crystal growth stops at the point of contact and no rods were found at −1.2 V, as shown in Fig. 2(f), which revealing the particle size about 50–150 nm. This may be the balancing effect of crystal growth against nucleation. At this voltage, it is also near the onset of H_2O reduction in reaction (5), and then OH^- is relatively increased to form more LiOH, resulting in space charge effect on SEM micrograph. At more negative voltage, the bubble effects were found on the surface of sample. This is because the rate of reaction (5) was increased with increasing applied voltage (or current density) and much more H_2 bubbles were produced. These results indicate that the morphology of the Sn/Li_2O coating film is highly dependent on the applied voltage during electro-deposition.

3.3. Crystal structures

The XRD diagram of various applied voltage specimens revealed Sn crystal, as shown in Fig. 3. This result supports reaction (3) proposed in region II. Fig. 3(a)–(f) shows the XRD pattern of Sn/Li_2O

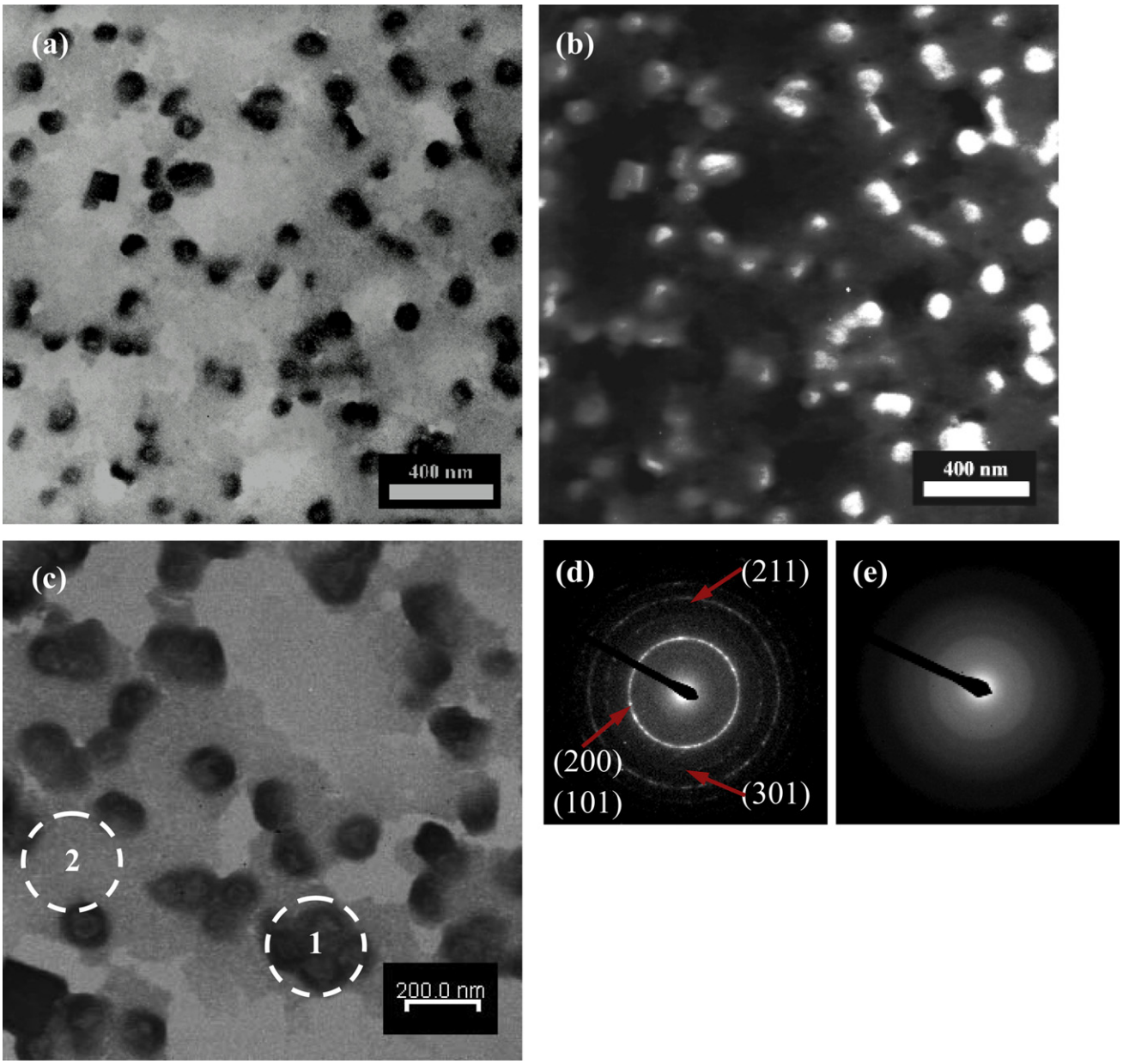

Fig. 5. TEM micrographs of the Sn/Li_2O films observed by at (a) bright field image, (b) dark field image, (c) higher magnification of bright field image, SAD (selected area diffraction) of (d) Sn particles, and (e) amorphous Li_2O area from zone 1 and zone 2 in (c), respectively.

thin films under different deposition potential. Deposition potentials will greatly affect the phase structural and morphological features of resulting Sn or Sn/Li_2O films. The major crystal structure showed (2 0 0), (1 0 1), (2 1 1), (3 0 1), (4 0 0), and (3 2 1) peaks of β-Sn due to Sn^{2+} in reaction (3) at applied voltage from −0.7 to −1.2 V. The intensity of diffraction peaks dropped abruptly at −1.2 V, since the micro-sized rods were not found. The peak of LiOH or Li_2O was never found in XRD patterns. Fig. 4 shows the XPS spectra of Li (1 s) for the Sn/Li_2O coating films deposited at (a) −1.0 and (b) −1.2 V, respectively. The peak at 55.3 eV of XPS spectra can be assigned to the Li^+ bonding in Li_2O. It is obvious that the intensity of Li (1 s) at −1.0 V (Fig. 4(a)) was much lower than that at −1.2 V. The more negative applied voltage, the more LiOH finally transformed into Li_2O was deposited since reaction (4) was increased with increasing applied voltage. However, it was not clear about the microstructure of Sn/Li_2O composite film. Therefore, TEM observations including bright field, dark field, and selected area diffraction (SAD) pattern were employed to discriminate Sn from Li_2O. Fig. 5(a) and (b) illustrate TEM bright field and dark field images of Sn and Li_2O, respectively. In the bright filed image, the dark particles were Sn, and the light gray area was Li_2O matrix. A higher magnification of Fig. 5(b) was shown in Fig. 5(c). The SAD pattern of regions 1 and 2 in Fig. 5(c) corresponded to Fig. 5(d) and (e), respectively. The SAD pattern of dark clusters in region 1 of Fig. 5(c) indicates that the dark clusters were β-Sn crystals. On the other hand, the diffraction rings for the gray region in Fig. 5(c) were diffusive. It is obvious that the gray region was amorphous Li_2O phase. In other words, Sn crystals were embedded in amorphous Li_2O matrix.

The XRD diffraction patterns of the as-deposited sample, annealed at 200, and 250 °C for 3 h, are shown in Fig. 6(a)–(c), respectively. There was no difference between Fig. 6(a) and (b). This indicates that no further significant crystallization occurred when the samples was heated at 200 °C. They both consisted of β-Sn phase and amorphous Li_2O, revealing β-Sn peaks of planes (2 0 0), (1 0 1), (2 1 1), (3 0 1), (1 1 2), and (4 0 0). When the temper-

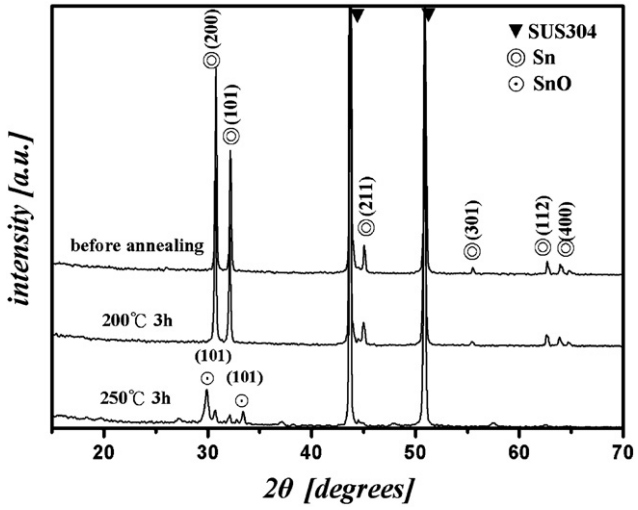

Fig. 6. XRD patterns of (a) the as-coated Sn/Li_2O films in solution E, and the post-annealed at (b) 200 °C, and (c) 250 °C for 3 h, respectively.

ature was raised to 250 °C, the oxidation of β-Sn in air was found, as shown in Fig. 6(c).

3.4. Electrochemical performances

Prior to fabrication, both Sn-coated and Sn/Li_2O-coated specimens were prepared by annealing at 200 °C for 3 h. The cyclic voltammograms (CV) of Sn and Sn/Li_2O recorded at a scan rate of 0.5 mV s^{-1} between 0.02 and 1.5 V are shown in Fig. 7(a) and (b). In the first cycle of Sn-coated specimen, four current peaks at 1.2, 0.6, 0.45, and 0.3 V were found during discharging, and the other five peaks at 0.5, 0.66, 0.75, 0.81, and 1.2 V during charging, as shown in Fig. 7(a). As in the literatures [22,23], it is well known that there is no formation of Li_xSn phases above 0.8 V for Sn electrodes. The low intensity of reduction peak at approximately 1.2 V disappears at second sweep. It is the typical phenomenon for the lithium alloy anodes, which corresponds to the formation of solid electrolyte interface (SEI) film on the surface of the active particles. The SEI film was formed leading to mostly irreversible capacity in the first cycle. The current peaks at 0.6, 0.45, and 0.3 V in the reduction process are caused by the formation of Li–Sn alloys. According to Huggins' report [22], these three peaks are related to formation of a Li-deficient phase (0.6 V) and a Li-rich phase (0.3 and 0.45 V). The CV curve of Sn/Li_2O coated was quite similar to Sn coated, as shown in Fig. 7(a) and (b).

Three corresponding charging–discharging plateaus were also found in the constant current chronopotentiometry, as shown in Fig. 8. Several plateaus at a Sn/Li_2O coating were due to the thermodynamical Sn–Li alloy and de-alloy reactions, and the discharge curve is similar to the early report [22]. During the first discharge, the irreversible capacity between the open-circuit potential and 0.7 V was about 144 mAh g^{-1}. It is well known that this is the formation of passivation films. The curve indicates three plateaus from 0.7 to 0.4 V and then gradually decline to the cut-off voltage of 0.02 V. The first plateau at 0.7 V corresponds to the following reaction

$$Sn \rightarrow Li_{0.4}Sn \quad (8)$$

The second plateau at around 0.52 V corresponds to the following reaction

$$Li_{0.4}Sn \rightarrow LiSn \quad (9)$$

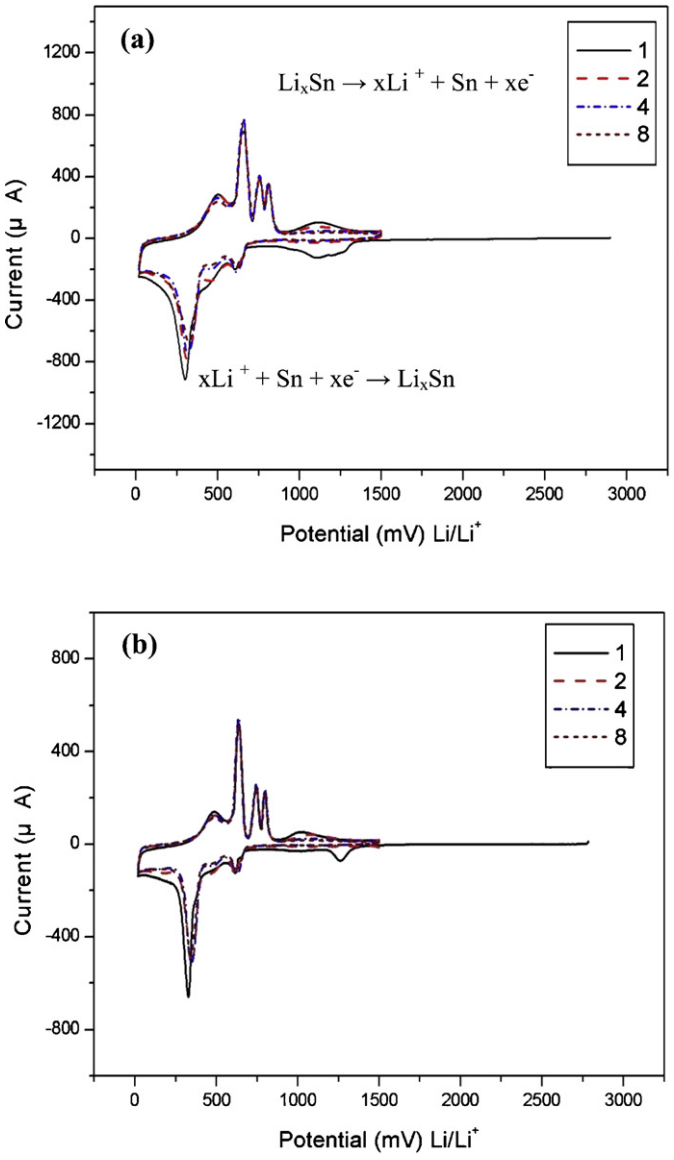

Fig. 7. Cyclic voltammograms of the (a) Sn-coated and (b) Sn/Li_2O coated specimens annealed at 200 °C in 1 M $LiClO_4$ electrolyte cells, the first one at a scanning rate of 0.5 mV s^{-1} between 2.7 and 0.02 V (Li/Li^+), and the subsequent ones between 1.5 and 0.02 V(Li/Li^+).

The third plateau at around 0.4 V corresponds to the following reaction

$$LiSn \rightarrow Li_{2.33}Sn \quad (10)$$

The gradual decreasing curve corresponds to the following reaction

$$Li_{2.33}Sn \rightarrow Li_{2.5}Sn \rightarrow Li_{2.6}Sn \rightarrow Li_{3.5}Sn \rightarrow Li_{4.4}Sn \quad (11)$$

Fig. 9 shows the discharge capacities of the Sn/Li_2O samples for different cut-off voltage ranges. The first discharge capacity of cut-off voltage about 1014, 1019, and 1161 mAh g^{-1} for cut-off voltage 0.9, 1.2, and 1.5 V, respectively. They were a little more than the theoretical capacity of Sn (991 mAh g^{-1}). The second discharge capacities were about 682, 705, and 762 mAh g^{-1} for cut-off voltage 0.9, 1.2, and 1.5 V, respectively. The irreversible capacities between the first and second discharge was about 300–400 mAh g^{-1}, as listed in Table 2. Beside the formation of passivation film, the obvious capacity loss between first and second discharge may be due to irreversible trap of Li^+ in crystal structure defects, such as vacancies, dislocations, and grain boundaries. Though the cut-off voltage

Table 2
Irreversible and reversible capacities of Sn/Li_2O for various cut-off voltages 0.9, 1.2, and 1.5 V shown in Fig. 9

Cut-off voltage	Initial capacity ($mAh\,g^{-1}$)	Capacity at cycle 2 ($mAh\,g^{-1}$)	Irreversible capacity ($mAh\,g^{-1}$)	Irreversible capacity (%)	Capacity at cycle 50 ($mAh\,g^{-1}$)	Capacity retention C50/C2 (%)
0.02–0.9 V	1004	682	322	32.1	587	86.1%
0.02–1.2 V	1019	705	314	30.8	448	63.5%
0.02–1.5 V	1161	762	399	34.3	374	49.1%

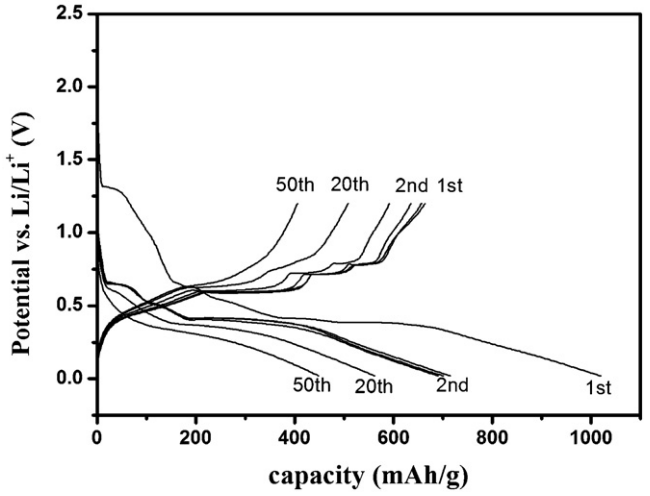

Fig. 8. Potenial profiles of Sn/Li_2O-coated specimens annealed at 200 °C in liquid electrolyte cells between 1.2 and 0.02 V (Li/Li^+) at 50 μA cm^{-2}.

at 0.9 V cannot offer a high enough over-potential, its cyclability is the best one among all. Its capacity for 50th cycle was around 587.5 mAh g^{-1} and the capacity retention ratio C50/C2 was about 81.6%, higher than 63.5% and 49.1% for the cut-off voltage at 1.2 and 1.5 V, as listed in Table 2. The lower cut-off voltage such as at −0.9 V means that the reverse reaction of (8) was not complete. In other words, the de-alloy reaction was not finished. The existence of $Li_{0.4}Sn$ might retard the agglomeration of Sn and the growth of particles. This argument was supported by the smaller particles for the cut-off voltage at 0.9 V, as shown in Fig. 10(a). On the other hand, the more agglomeration of particles were found at 1.2 and 1.5 V, as shown in Fig. 10(b) and (c). Finally, the agglomeration of particles increased the diffusion length of Li^+ and reduced

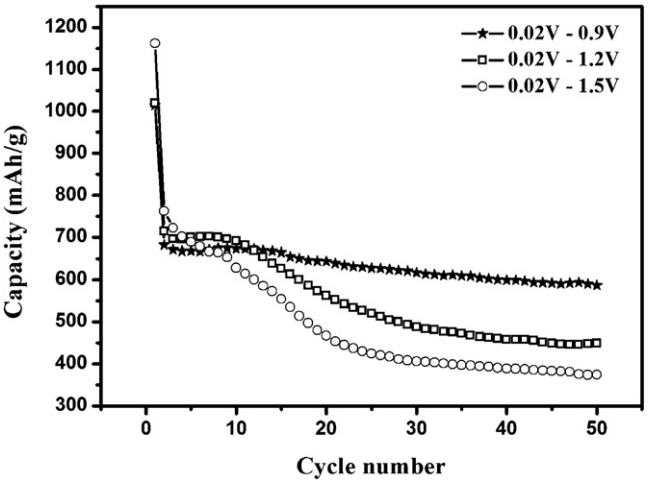

Fig. 9. The evolution of discharge capacity vs. the cycle number for Sn/Li_2O film annealed at 200 °C in 1 M $LiClO_4$ electrolyte at 50 μA cm^{-2} from 0.02 V to cut-off voltages 0.9, 1.2, and 1.5 V (Li/Li^+).

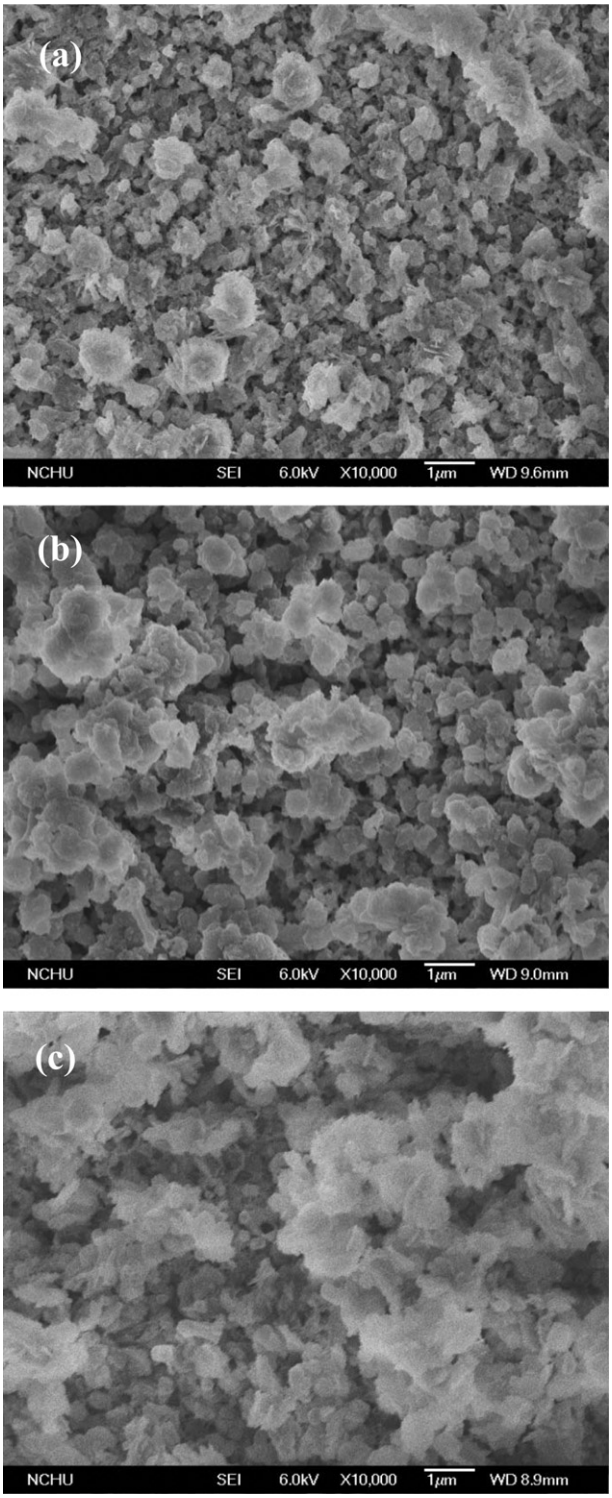

Fig. 10. FE-SEM observations of the coated specimen annealed at 200 °C after the 50th cyclic test from 0.02 V to cut-off voltages (a) 0.9, (b) 1.2, and (c) 1.5 V (Li/Li^+).

Table 3
Cycling performances of electrolytic Sn/Li_2O coating in this study compared with sputtered Sn, SnO_2, and Sn/Li_2O coatings.

	Initial capacity ($mAh\,g^{-1}$)	Capacity at cycle 2 ($mAh\,g^{-1}$)	Irreversible capacity ($mAh\,g^{-1}$)	Irreversible capacity (%)	Capacity at cycle 50 ($mAh\,g^{-1}$)	Capacity retention C50/C2 (%)
Sn [14]	997	624	373	37.4	335	53.7
Sn [15]	963	744	219	22.7	432	58.1
SnO_2 [21]	1370	500	870	63.5	180	36
SnO_2 [24]	1494	490	1004	67.2	–	–
Sn/Li_2O [20]	1050	520	530	50.4	440	84.6
This study	1004	682	322	32.1	587	86.1

the reversibility. Reversible capacity of Sn/Li_2O coating for cut-off voltage at 1.2 and 1.5 V was rapidly decreased with increasing of cycle number during 20 cycles as shown in Fig. 9. Larger Sn particles were more sensitive to cracking and crumbling due to larger absolute volume changes than smaller particles [23]. Besides, the electrolytic Sn/Li_2O composite film revealed higher capacity at 2nd and 50th cycles and lower irreversible capacity than that prepared by sputtering [20]. Comparing Sn [14,15], SnO_2 [21,24], and Sn/Li_2O (≈185 $\mu g\,cm^{-2}$) [20] coatings, the reversible capacities of electrolytic Sn/Li_2O coating (≈120 $\mu g\,cm^{-2}$) was higher than the others, as listed in Table 3. The better cycle retention of Sn/Li_2O than that of Sn can be attributed that Li_2O has a glue function that can adhere other particles. Also the Li_2O matrix can retard the further agglomeration of Sn particles, resulting in much better cycling characteristics. Obviously, the electrolytic method presented in this study is very promising for application in lithium-ion thin-film batteries.

4. Conclusions

Electrolytic deposition method combining annealing has been successfully used to fabricate Sn/Li_2O thin-film electrodes for Li batteries in 1 mM $SnCl_2$ and 0.1 M $LiNO_3$ mixed solution. It was found that the cathodic polarization curves should be divided into three regions: (I) $O_2 + 4H^+ + 4e^- \rightarrow 2H_2O$ (~0.25 to −0.5 V), (II) $2H^+ + 2e^- \rightarrow H_2$, $Sn^{2+} + 2e^- \rightarrow Sn$, and $NO_3^- + H_2O + 2e^- \rightarrow NO_2^- + 2OH^-$ (−0.5 to −1.34 V), (III) $2H_2O + 2e^- \rightarrow H_2 + 2OH^-$ (−1.34 to −2 V vs. Ag/AgCl). The more efficient deposition was found nearby to the lower part of region II, because much more OH^- ions were produced and more Li^+ ions migrated to the cathode to from LiOH. LiOH was condensed into amorphous Li_2O by subsequently annealing. Also, morphology of the Sn/Li_2O coating film is highly dependent on the applied voltage during electro-deposition. Only micro-sized Sn rods were observed at −0.7 and −0.8 V, and nano-sized round Sn particles embedded in amorphous Li_2O matrix at −1.0 to −1.2 V. Amorphous Li_2O matrix revealed the retarding effects on the further agglomeration of Sn particles and resulting in much better cycling characteristics. The incomplete de-alloy for cut-off voltage at 0.9 V (vs. Li/Li^+) resulting in the retained $Li_{0.4}Sn$ might further retard the coarsening Sn particles, finally revealing reversible capacity 587.5 $mAh\,g^{-1}$ and capacity retention ratio C50/C2 about 81.6%, which was higher than 63.5% and 49.1% for cut-off voltages at 1.2 and 1.5 V.

Acknowledgments

The authors are grateful for the support of this research by the National Science Council, and the Department of Industrial Technology, Ministry of Economic Affairs, Republic of China under contract no. NSC 96-2222-E-005-001-CC3, and no. 97-EC-17-A-31-R8-0737-2, respectively.

References

[1] T.D. Tran, J.H. Feikert, X. Song, K. Kinoshita, J. Electrochem. Soc. 142 (1995) 3297–3302.
[2] Y. Idota, US Patent 5478671 (1995).
[3] H. Tomyama, Jpn. Patent 07-029608 (1995).
[4] I.A. Courtney, J.R. Dahn, J. Electrochem. Soc. 144 (1997) 2943–2948.
[5] I.A. Courtney, W.R. McKinnon, J.R. Dahn, J. Electrochem. Soc. 146 (1999) 59–68.
[6] Y. Idota, T. Kubota, A. Matsufuji, Y. Maekawa, T. Miyasaka, Science 276 (1997) 1395–1397.
[7] J.O. Besenhard, J. Yang, M. Winter, J. Power Sources 68 (1997) 87–90.
[8] C.S. Wang, John Appleby, A. Frank, E. Little, J. Power Sources 93 (2001) 174–185.
[9] R.A. Huggins, Solid State Ionics 113–115 (1998) 57–67.
[10] J.O. Besenhard, M. Wachtler, M. Winter, R. Andreaus, I. Rom, W. Sitte, J. Power Sources 81–82 (1999) 268–272.
[11] Y.S. Fung, D.R. Zhu, J. Electrochem. Soc. 149 (2002) A319–A324.
[12] G.M. Ehrlich, C. Durand, X. Chen, T.A. Hugener, F. Spiess, S.L. Suib, J. Electrochem. Soc. 147 (2000) 886–891.
[13] O. Mao, J.R. Dahn, J. Electrochem. Soc. 146 (1999) 414–422.
[14] K.F. Chiu, H.C. Lin, K.M. Lin, T.Y. Lin, D.T. Shieh, J. Electrochem. Soc. 153 (2006) A1038–A1042.
[15] K.F. Chiu, H.C. Lin, K.M. Lin, T.Y. Lin, D.T. Shieh, J. Electrochem. Soc. 153 (2006) A920–A924.
[16] W. Choi, J.Y. Lee, B.H. Jung, H.S. Lim, J. Power Sources 136 (2004) 154–159.
[17] T. Zhang, L.J. Fu, J. Gao, Y.P. Wu, R. Holze, H.Q. Wu, J. Power Sources 174 (2007) 770–773.
[18] Y.N. Nuli, S.L. Zhao, Q.Z. Qin, J. Power Sources 114 (2003) 113–120.
[19] S.T. Chang, I.L. Leu, M.H. Hon, Electrochem. Solid-State Lett. 5 (2002) C71–C74.
[20] S.C. Nam, Y.S. Yoon, W.I. Cho, B.W. Cho, H.S. Chun, K.S. Yun, Electrochem. Commun. 3 (2001) 6–10.
[21] J.J. Lee, S.H. Kim, S.H. Jee, Y.S. Yoon, W.I. Cho, S.J. Yoon, J.W. Choi, S.C. Nam, J. Power Sources 178 (2008) 434–438.
[22] M. Winter, J.O. Besenhard, Electrochim. Acta 45 (1999) 31–50.
[23] R.A. Huggins, J. Power Sources 81/82 (1999) 13–19.
[24] W.H. Ho, H.C. Liu, H.C. Chen, S.K. Yen, Surf. Coat. Technol. 201 (2007) 7100–7106.